Mössbauer data analysis based on invariants and application to UFe_5Sn

D. Satuła,[1] K. Szymański,[1] L. Dobrzyński,[1,2] V. H. Tran,[3] and R. Troć[3]
[1]*University of Białystok, Faculty of Physics, Lipowa 41, 15-424 Białystok, Poland*
[2]*The Soltan Institute of Nuclear Studies, 05-400 Otwock-Świerk, Poland*
[3]*W. Trzebiatowski Institute of Low Temperature and Structure Research, Polish Academy of Sciences, P.O. Box 1410, 50-950 Wrocław, Poland*
(Received 11 March 2008; revised manuscript received 7 May 2008; published 7 July 2008)

A method for Mössbauer data treatment is proposed for texture-free samples. Parameters of hyperfine interactions, Debye temperature, temperature dependence of the electric-field gradient components, site occupancies, and magnetic moments of the ground state are measured for UFe_5Sn. Spin reorientation is evidenced and anomalous temperature dependence of magnetic moments at specific sites is revealed. The presented results do not contain full information about parameters of hyperfine interactions but are free of ambiguity typical for 3/2–1/2 nuclear-spin transitions because only experimentally available information is being considered. It is proven that the presented method could be easily employed with the help of widely used standard Mössbauer packages when some constraints are applied.

DOI: 10.1103/PhysRevB.78.014411 PACS number(s): 75.25.+z, 76.80.+y, 75.50.Bb, 71.20.Lp

I. INTRODUCTION

It was recognized already in the 1960's that details of the hyperfine structure cannot be unambiguously determined from the Mössbauer spectrum of a randomly oriented, thin absorber in which mixed interactions (e.g., magnetic dipole and electric quadrupole) are present.[1] This limitation applies even to the simplest case of a single site and is called the ambiguity problem.[2–5] Application of the external magnetic field,[6] use of single crystals,[7] or polarimetric methods[8,9] are helpful issues in the complete determination of the hyperfine interactions. More serious problem arise when many sites are present or when distribution of hyperfine interactions causes an overlap of the absorption lines.[10,11]

Although the randomly oriented absorber information obtained by Mössbauer spectroscopic methods is poorer than in the case of using single crystals, obviously the availability of powders and difficulties in some single-crystal growth make the use of powdered absorbers still highly desirable. Thus, the ambiguity problem has to be properly treated. This paper demonstrates an effective method of Mössbauer data treatment, applied to the particular case of a UFe_5Sn intermetallic alloy. An additional advantage of the presented method stems from the possibility of using (under proposed interpretation) the results obtained by standard Mössbauer packages equipped in full Hamiltonian formalism.

This paper is organized as follows. We present exact, explicit solutions for the positions and amplitudes of absorption lines in the case of 3/2–1/2 mixed transitions. Next, it is shown how to obtain a set of all possible hyperfine parameters, which realizes the specific absorption spectrum. The shape of the spectrum is given by a set of invariants. Then we show how to find the set and how to easily find its representation by the parameters of hyperfine interactions. Finally, the method is applied to the analysis of experimental data of UFe_5Sn. Spin reorientation in this compound is clearly evidenced by a discontinuity in the temperature dependence of invariants.

II. INVARIANTS IN THE CONTEXT OF THE AMBIGUITY PROBLEM

Line positions in the Mössbauer spectra are calculated by diagonalization of the spin-Hamiltonian matrix, while line amplitudes are given by a product of the eigenstates.[12] Since one has to deal with 4×4 matrices, the discussion of the spin Hamiltonian of the eigenvalues and thus line intensities is rather difficult for spin 3/2. We have shown in Ref. 13 that the concept of the intensity tensor[14–17] leads to the line intensities, which are given explicitly by scalars S_0, S_1, and S_2, constructed from the electric-field-gradient (EFG) tensor $\boldsymbol{V}$ and hyperfine magnetic-field (hmf) pseudovector $\boldsymbol{B}$:

$$S_0 = a\sqrt{\mathrm{Tr}\ \boldsymbol{V}^2},$$

$$S_1 = a\boldsymbol{m}^T\cdot\boldsymbol{V}\cdot\boldsymbol{m},$$

$$S_2 = a\sqrt{\boldsymbol{m}^T\cdot\boldsymbol{V}^2\cdot\boldsymbol{m}}, \tag{1}$$

where

$$a = eQc/E_\gamma \tag{2}$$

is the proportionality constant between EFG components [in $(\mathrm{V/m^2})$ SI units] and invariants expressed conveniently for applications in (mm/s). Q is the nuclear quadrupole moment, e is the elementary charge, c is the speed of light, and E_γ is the energy between the ground and the excited state ($\approx$14.4 keV). In Eq. (1), $\boldsymbol{m}=\boldsymbol{B}/B$ (B is the modulus of $\boldsymbol{B}$) is the unit vector parallel to $\boldsymbol{B}$.

The invariants S_0, S_1, and S_2 (or Tr $\boldsymbol{V}^2$, $\boldsymbol{m}^T\boldsymbol{V}\boldsymbol{m}$, and $\boldsymbol{m}^T\boldsymbol{V}^2\boldsymbol{m}$) have a clear physical interpretation. In Eq. (1), $6^{-1/2}S_0$ appears to be equal to $aV_{zz}(1+\eta^2/3)^{1/2}/2$ and would be just a separation between $I_e=3/2$ nuclear sublevels when the hmf is zero, or would be a separation between the absorption lines in the paramagnetic state. The asymmetry parameter η has the common meaning, i.e., defined by the diagonal components of the $\boldsymbol{V}$: $\eta=(V_{xx}-V_{yy})/V_{zz}$. The diagonal components V_{ii} are chosen so that $|V_{xx}|\leq|V_{yy}|\leq|V_{zz}|$, resulting in $0\leq\eta\leq1$.

$\boldsymbol{m}^T\boldsymbol{V}\boldsymbol{m}$ is the component of the EFG tensor $\boldsymbol{V}$ in the direction of the hmf, and its sign may be positive or negative. The average value of $\boldsymbol{m}^T\boldsymbol{V}\boldsymbol{m}$ [when $\boldsymbol{m}$ is randomly oriented in the principal-axis system (PAS) of the $\boldsymbol{V}$] is zero.[18] S_1 is proportional to the shift of the absorption lines 2, 3, 4, 5 with respect to the 1 and 6 in the Zeeman sextet caused by a small quadrupole interaction in the first-order approximation.[19]

The invariant $\boldsymbol{m}^T\boldsymbol{V}^2\boldsymbol{m}$ is the component of the $\boldsymbol{V}^2$ in the direction of the hmf, $V_{zz}^2(1-\eta)^2/4 \le \boldsymbol{m}^T\boldsymbol{V}^2\boldsymbol{m} \le V_{zz}^2$. It also shows the length of $\boldsymbol{V}\boldsymbol{m}$. Indeed, $\boldsymbol{m}^T\boldsymbol{V}^2\boldsymbol{m} = (\boldsymbol{V}\boldsymbol{m})\cdot(\boldsymbol{V}\boldsymbol{m})$. Some additional properties of invariants [Eq. (1)] are given in the Appendix. Finally, it should be noted that the choice of the invariants [Eq. (1)] is not unique.

Some results from Ref. 13 are essential to the present considerations, and are recalled as follows. The secular equation for the eigenvalues E of the excited $I_e=3/2$ state is

$$\lambda^4 + p\lambda^2 + q\lambda + r = 0,$$

$$\lambda = 2E/v_B, \tag{3}$$

where $v_B = g_{3/2}\mu_N Bc/E_\gamma$ is the Zeeman splitting between $I_e=3/2$ sublevels expressed in velocity units, μ_N is the nuclear magneton, and $g_{3/2}$ is the nuclear g-factor of the excited state. The coefficients p, q, and r are

$$p = -10 - \frac{1}{3}(S_0/v_B)^2,$$

$$q = -8S_1/v_B,$$

$$r = \frac{1}{4}(p+4)^2 - 4(S_2/v_B)^2. \tag{4}$$

The absorption line intensity for a randomly oriented absorber in the case of a $3/2 \rightarrow 1/2$ magnetic dipolar transition is proportional to the trace of the intensity tensor $\boldsymbol{I}_{\alpha\beta}$, and the explicit form is (Ref. 13)

$$\mathrm{Tr}\ \boldsymbol{I}_{\alpha\beta} = \frac{3}{8} + \beta\frac{40\lambda_\alpha^2 - 4q\lambda_\alpha + (p+4)(p+16) - 4r}{16(4\lambda_\alpha^3 + 2p\lambda_\alpha + q)}. \tag{5}$$

The index $\beta = \pm 1$ corresponds to two ground states, while four eigenvalues λ_α are roots of secular Eq. (3).

The explicit form of the roots can be found in Ref. 18. The line positions $v_{\alpha\beta}$ (expressed conveniently in the velocity units) are

$$v_{\alpha\beta} = (\lambda_\alpha - \beta g_{1/2}/g_{3/2})v_B/2, \tag{6}$$

where $g_{1/2}$ is the nuclear g-factor of the ground state.

The results [Eqs. (1), (5), and (6)], fully determining the absorption line positions and intensities, depend on four invariants only: B, S_0, S_1, and S_2, while there are five independent hyperfine parameters: B, θ, φ, V_{zz}, and η, where θ and φ are polar and azimuthal angles of the $\boldsymbol{B}$ vector in PAS of the $\boldsymbol{V}$ tensor.

It would be helpful to consider a typical example (for instance, assuming no accidental relations between parameters), which illustrates the ambiguity problem. Let us take $eQcV_{zz}/E_g = -2$ mm/s, $B = |eQV_{zz}/(4g_{3/2}\mu_N)|$ (=7.364…T),

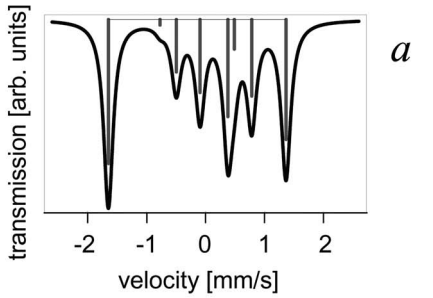

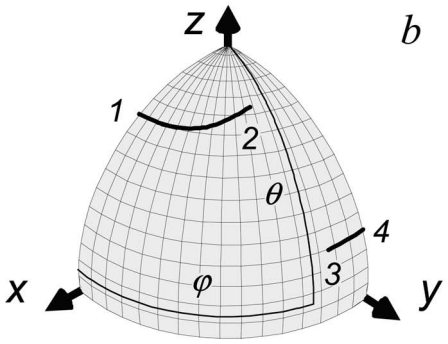

c

no	R	η	θ	φ
1	2.152	0.278	0.588	0.000
2	1.887	1.000	0.455	1.047
3	-1.887	1.000	1.181	1.331
4	-1.947	0.872	1.171	1.571

FIG. 1. (a) Simulated Mössbauer absorption spectrum for hyperfine field $B = |eQV_{zz}/(4g_{3/2}\mu_N)|$ (=7.3641 T), and invariants S_0, S_1, and S_2 (1) equal to $(57/8)^{1/2}$, $-5/4$, $(217/64)^{1/2}$ (all in mm/s), respectively. (b) Thick lines drawn on part of the unit sphere show possible values of the polar θ and azimuthal φ angles of the $\boldsymbol{B}$ vector in the principal axes system of the electric-field-gradient tensor $\boldsymbol{V}$. At some points marked by numbers 1, 2, 3, 4, (c) values of the main diagonal component V_{zz} [$R = eQV_{zz}/(2g_{3/2}\mu_N$, see text after Eqs. (1) and (3) for explanation of the symbols], the asymmetry parameter η and angles θ and φ are given in the table. For all points located on the thick lines, the values of the invariants do not change. This means that the spectrum shown in (a) remains unchanged.

$\eta = 3/4$, $\theta = \pi/6$, and $\varphi = \pi/4$. So, S_0, S_1, and S_2 invariants [Eq. (1)] are equal to $(57/8)^{1/2}$, $-5/4$, $(217/64)^{1/2}$ (all in mm/s), respectively. The line positions [Eq. (6)] and intensities [Eq. (5)] as well as the absorption spectrum are shown in Fig. 1(a). In Fig. 1(b), as thick lines, we show all possible values of the V_{zz}, η, θ, and φ for which the invariants S_0, S_1, and S_2 and thus the spectrum remains unchanged. For clarity, only $0 \le \theta \le \pi/2$ and $0 \le \varphi \le \pi/2$ are shown in Fig. 1(b). Other values, such as V_{zz}, η, θ, and φ, can be obtained by mirror reflections with respect to the xy, xz, and yz planes in the PAS of the $\boldsymbol{V}$ tensor. Some numerical values, such as V_{zz}, η, θ, and φ, are given in Fig. 1(c).

Two important specific cases (e.g., for special choice of the hyperfine parameters) have to be mentioned. (i) If $\eta = 0$,

the problem has axial symmetry, and thus, in Fig. 1(b), there are additional circles (θ=const, $0 \leq \varphi \leq 2\pi$). (ii) If in the considered case of axial symmetry the angle θ is a magic angle, i.e., $\cos\theta = 3^{-1/2}$, all invariants [Eq. (1)] expressed by $(V_{zz}, \eta, \theta, \varphi)$ will not contain terms linear in V_{zz}, thus making the determination of the sign of V_{zz} impossible. In that case, the pair of circles (for $\pm V_{zz}$) would overlap in Fig. 1(b).

III. PRINCIPLES OF DATA TREATMENT BASED ON THE INVARIANTS METHOD

Because line intensities and their positions are fully determined by four invariants: B, S_0, S_1, and S_2, it is obvious that only these values (or their functions) could be extracted if no other information is available. Thus, it would be desirable to have a method in which fitted or simulated parameters were expressed in terms of B, S_0, S_1, and S_2. In principle, one can construct such a routine based on Eqs. (1), (5), and (6), however, we propose a more convenient solution. The observation is that the thick lines, which show possible values of φ and θ [Fig. 1(b)] for constant values of B, S_0, S_1, and S_2, always cross the meridian $\varphi=0$ or $\varphi=\pi/2$, or equator $\theta=\pi/2$. This is quite a general situation, which is shown in the Appendix. Thus, one could use standard fitting packages, which properly treat mixed interactions, and in order to find hyperfine parameters describing the experimental data, one must check all possibilities related to the main meridians and the equator. By doing so, e.g., traveling on the main meridians and the equator with the angles θ and φ, we are sure of probing all possibilities of S_0, S_1, and S_2 invariants (see the Appendix for a mathematical proof).

IV. PROPERTY OF INTERMETALLIC UFe_5Sn COMPOUND

The intermetallic compound UFe_5Sn, discovered by Gonçalves *et al.*,[20] crystallizes in an orthorhombic $CeCu_5Au$-type structure (space group Pnma). The unit cell contains 4 U atoms located on the 4*c* site, 4 Sn atoms on 4*c*, 8 Fe atoms on 8*d* (Fe1), and 12 Fe atoms on 4*c* (Fe2, Fe3, and Fe4) sites.[20] The relative populations of the iron atoms at the four different sites fulfill the 2:1:1:1 ratio. The iron atoms Fe1 and Fe3 have identical chemical nearest surroundings (3 uranium, 2 tin, 7 iron atoms), however, they differ by the arrangement of atoms. The surroundings of Fe2 and Fe4 are (3 uranium, 3 tin, 5 iron atoms) and (3 uranium, 1 tin, 8 iron atoms), respectively. According to magnetization data performed on a powder sample, UFe_5Sn shows a weak ferromagnetic behavior at room temperature and undergoes two magnetic transitions at 248 and 180 K.[20] The latter transition was reported to be magnetic-field dependent and disappears for $B_{ext} > 1$ T. It was reported also that the magnetization below 248 K strongly increases with decreasing temperature. More precise experiments on a single crystal[21] have revealed that the transition at 248 K is associated with the ferromagnetic ordering of iron magnetic moments along the *c* axis, while anomalies observed at 180 K are associated with reorientation of Fe moments toward the *b* axis. This conclusion was deduced partially from Mössbauer measurements. However, in our opinion, a more exact description of the UFe_5Sn spectra can be obtained by using the mixed hyperfine interactions instead of the first-order perturbation theory presented in Ref. 21. Since the electric quadrupolar interactions are not small with respect to the magnetic dipolar ones, the full Hamiltonian should be used for a correct description of the Mössbauer spectra.

An important initial step in the analysis involves the determination of the temperature behavior of parameters of hyperfine interactions expressed by invariants, which may describe properly the experimental Mössbauer spectrum.

V. SAMPLE PREPARATION

A single crystal of UFe_5Sn was grown by the Czochralski method. The sample characterization is given elsewhere.[22] The powdered sample studied in this work was made by crushing part of a large single crystal, and the obtained powder was mixed with both Li_2CO_3 and epoxy glue. Such a preparation ensures the random distribution of the grains, resulting in a texture-free sample. The sample thickness used in our experiment was 12 mg UFe_5Sn per cm^2.

VI. MÖSSBAUER MEASUREMENTS AND QUALITATIVE DESCRIPTION OF THE SPECTRA

Mössbauer measurements at various temperatures were carried out in a closed-cycle refrigerator equipped with an antivibration shroud. The source of radiation was ^{57}Co in a Cr matrix. The velocity scale was calibrated with respect to α-Fe at room temperature.

All spectra were analyzed initially by a commercial Mössbauer package "Normos" using a transmission integral.[23] Recoilless fraction of Fe atoms in UFe_5Sn was assumed to be the same as in α-Fe.[24] The resulting values of the effective thickness of the absorber extrapolated to $T=0$ was estimated to be $\tau = 2.41 \pm 0.11$.

The Mössbauer spectrum measured at room temperature was fitted using two doublets with the same values of the width of the Lorentzian lines $[D(1), D(2)]$, shown on the top of Fig. 2. The ratio of the areas of these two doublets is close to four, consistent with an assumption that a stronger doublet $D(1)$ is created by 8 Fe atoms at 8*d* and by 8 Fe atoms at 4*c* sites, while the $D(2)$ doublet is created by 4 Fe atoms at the 4*c* site. The difference of the isomer shift (IS) between the $D(2)$ and $D(1)$ doublets is 0.18 mm/s. Because the Sn atoms located in the nearest neighborhood (NN) of Fe should increase its IS,[25] the $D(2)$ doublet must be ascribed uniquely to the Fe2 site, which has three Sn atoms in the NN shell; NNs are located at distances ranging from 2.61 to 2.93 Å.[20] However, the overall situation may be more complicated. In particular, the Fe4 site has only one atom Sn in NN, with an interatomic distance of 2.77 Å, and no extra doublet connected with this site is resolved in the measured spectrum. The absorption lines are almost not broadened (their widths are almost equal to the widths of the lines in the calibration spectrum of α-Fe). It is puzzling that three different sites (Fe1, Fe3, and Fe4) could be fitted by a single doublet. We will show in Sec. VII that some reasonable assumption about

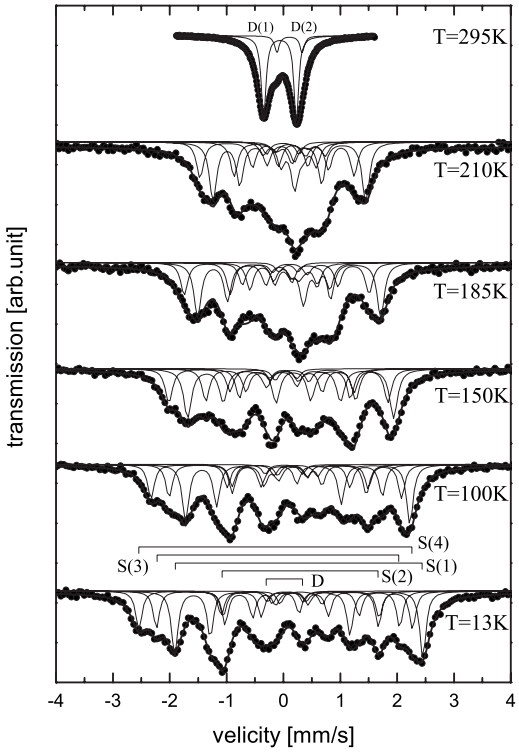

FIG. 2. Selected Mössbauer spectra taken at different temperatures. Solid lines represent the best simultaneous fit described in Sec. VIII.

temperature dependences of hyperfine interactions leads to the conclusion that these three sites have in fact slightly different parameters of hyperfine interactions, and the proposed method of invariants allows us to derive these parameters.

The selected Mössbauer spectra measured in the temperature range 13–295 K are presented in Fig. 2. The spectra from room temperature down to 250 K contain doublets only.

At $T=240$ K, the spectrum starts to broaden, indicating that from room temperature down to 240 K, the magnetic hyperfine field is equal to zero and the iron ions are in the paramagnetic state. The temperature where the broadening of the doublet is observed corresponds well with the first transition temperature previously reported in the magnetization measurements.[20] The spectra taken between 240 and 13 K exhibit a complicated magnetically split pattern, whose behavior must be connected with the four different local iron surroundings. The local values of the hmf gradually increase with decreasing temperature.

VII. RESULTS OF ANALYSIS WITH UNCONSTRAINED INVARIANTS METHOD

An initial analysis of the magnetically split spectra measured at 13 K was done using a full Hamiltonian and fitting four magnetic components $S(n)$ $(n=1,2,3,4)$, and one doublet (D) located in the central part of spectra, all exhibiting very sharp lines (the width of the lines connected with the absorber is $\Gamma_a=0.13\pm0.01$ mm/s). Each sextet was fitted as described in Sec. III, and we were able to find the set of the invariants, which describe well the measured spectrum. Because the population of Fe at the 8*d* sites should be two times larger than those of the remaining sites, one expects that the most intense component $S(1)$ corresponds to the Fe1 site. Assuming that the hmf of Fe increases with the number of Fe atoms in the NN, such as in the case of U-Fe-Al (Ref. 26) and in Fe-Sn (Ref. 27) systems, one suspects that $S(2)$, $S(3)$, and $S(4)$ come from the Fe2, Fe3, and Fe4 sites, respectively. This conjecture is consistent with that reported in Ref. 21 and agrees well with the identification of the NN surrounding the small doublet observed in room-temperature data. However, in contrast to the previous results,[21] the relative area under the doublet D observed at low temperatures is two times smaller than that of the sextet ($B_{hf}=2$ T).[21] Because its relative area is small, the origin of this doublet is not clear at present. Nevertheless, a comparison of the hyperfine parameters obtained here indicates that the value of IS for the doublet D is close to that of the $S(3)$ component, which in turn implies that this doublet can be rather associated with the Fe3 site. However, it is difficult to understand why part of the iron atoms at the Fe3 site should be paramagnetic at $T=13$ K. Therefore, it seems more likely that the considered doublet results from a small fraction of Fe atoms located at an antisite positions, U, or Sn atoms. Two additional features, evidenced in the change in shapes of measured spectra, should be noticed.

The first important feature is visible on the left-hand side of the spectra measured at 13, 100, and 150 K shown in Fig. 2. The change in the first three lines located at velocities −2.6, −2.2, and −2.0 (mm/s, $T=13$ K) are attributed to the Fe4, Fe3, and Fe1 surroundings. The visible sequence of the intensities of respective lines at $T=13$ K and 100 K is: small, small, and large. If one looks at the spectrum obtained at $T=150$ K, this sequence is different: small, large, and small. This situation might occur if the hmf of the component due to the Fe3 surrounding decreases much faster with increasing temperature than the B_{hf} intensity of Fe1 and Fe4 sites.

The second feature visible in the change of spectral shapes appears between 150 and 185 K. The singlelike line seen in the central part of the spectra (at $v=0.3$ mm/s) at 185 K (Fig. 2) disappears at 150 K. Assuming that the EFG in metals is rather slightly dependent on temperature, a strong rearrangement of the line positions and the change in intensities are then presumably associated with a strong change of the direction of local magnetic moments in the PAS of the EFG for at least one iron position.

VIII. RESULTS OF SIMULTANEOUS FITS WITH CONSTRAINED INVARIANTS

Using invariants, we were able to find reasonably good fits to the spectra measured at low temperatures, where many absorption lines were narrow and relatively well separated. At temperatures higher than $T=200$ K, the spectra are strongly collapsed and there is a little hope for their proper decomposition. In this situation, we decided to fit simultaneously all measured spectra under some constraints stemming from physics of the problem:

(i) The relative intensities of the local components were kept constants for all spectra;

TABLE I. The local invariants $(6^{-1/2}S_0, S_1, S_2)$, isomer shift (IS), and relative intensities extrapolated to $T=0$ K. The last row shows the site occupancies resulting from the crystal structure.

	$S(1)$	$S(4)$	$S(3)$	$S(2)$	D
IS (mm/s)	0.113 ± 0.005	0.078 ± 0.005	0.052 ± 0.03	0.23 ± 0.01	0.08 ± 0.01
$6^{-1/2}S_0$ (mm/s)	0.74	0.68	0.67	0.50	0.65
S_1 (mm/s)	0.8	−0.9	−0.5	0.52	—
S_2 (mm/s)	1.02	1.06	0.71	0.91	—
hmf (T)	13.3 ± 0.2	14.9 ± 0.2	13.1 ± 0.3	8.1 ± 0.2	0.0
I (%)	33 ± 2	23 ± 2	23 ± 4	17 ± 4	4 ± 3
$I_{\text{cryst.str.}}$ (%)	40	20	20	20	

(ii) the temperature behavior of the second-order Doppler (SOD) shift was approximated by the Debye model with the same value of the characteristic temperature for all iron sites;

(iii) the $T^{3/2}$ law for the EFG components was assumed. The experimental fact is that the temperature dependence of the EFG in various noncubic metals is approximated reasonably well by $V_{ij}(T)=V_{ij}(0)(1-AT^{3/2})$, which results from the mean-square displacement of the host atoms.[28]

The best results of simultaneous fit to all the spectra are presented in Fig. 2 by solid lines for all performed temperature measurements. The measured spectra are described very well although there are small misfits in the central part of spectra. The hyperfine parameters extrapolated to $T=0$ K are presented in Table I. The values of hyperfine parameters of the ground state presented can be directly compared with electronic structure calculations. The behavior of the isomer shift (and SOD shift) and hmf versus temperature are presented in Figs. 3(a) and 3(b), respectively. As one can see, the results of the IS can be divided into two groups. The surrounding of the Fe2 has clearly higher values of IS than those of the three remaining sites (Fe1, Fe3, and Fe4). If one considers the composition the NN. thus one can conclude that the increase in the IS of Fe2 sites is connected with a higher number of Sn atoms in the NN. The Sn atoms as a NN increase the value of the IS observed in the Fe nuclei.[25] In spite of that, such an influence is not visible on the Fe4 atoms that have only one Sn atom in the NN. Moreover, in spite of similar composition of the NN, the IS for Fe1 and Fe3 is different. It means that the IS depends not only on the composition of the NN but also on other factors, such as the symmetry and the local distances of the NN atoms. The Debye temperature that corresponds to the SOD shift shown in Fig. 3(a) is equal to (301 ± 10) K for all types of surroundings, in agreement with the value previously obtained by Gonçalves *et al.*[21] The observed value is in the range typical for so-called 151 uranium compounds, UCu_5Al (329 K) (Ref. 29) and UCu_5Sn (250 K).[30]

The temperature dependence of the local hmf is presented in Fig. 3(b). The onset of the nonzero hmf is visible slightly below 250 K, which agrees well with the temperature of the first transition observed in the magnetization measurements. Moreover, the unusual behavior of hmf of Fe3 is clearly observed. Its hmf decreases apparently faster than the hmf of the remaining components. The fastest decrease in the hmf for Fe3 is observed when the temperature approaches 170 K, where the second anomaly was observed.[20,21] In addition, one can see that the hmf of Fe1 and Fe4 have different values at $T=13$ K, and they become almost equal to each other at $T=170$ K.

The dependence of the local hyperfine field extrapolated to $T=0$ K on the number of iron atoms located in NN show an almost linear relation between these two quantities. The Fe atom in the NN increases the hmf by (2.3 ± 0.2) T.

Let us estimate the local iron magnetic moments at the ground state on the basis of the hmf extrapolated to $T=0$ K. In order to do that, one has to estimate the coupling constant between the hmf and iron magnetic moment on the basis of neutron and Mössbauer results for a similar class of compounds. One of the best choices is UFe_4Al_8, which crystallizes in the tetragonal $ThMn_{12}$-type structure and under-

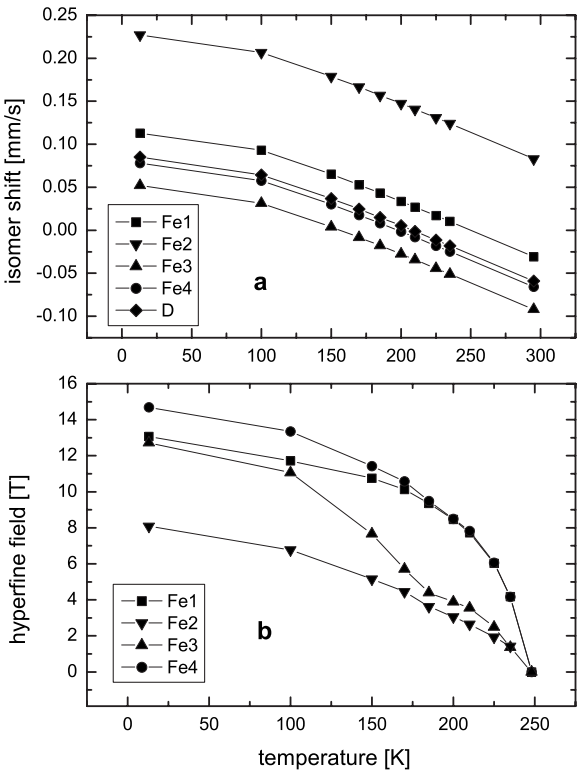

FIG. 3. The local isomer shift (a) and hyperfine magnetic field (b) vs temperature. The points on the isomer shift are calculated from the Debye model. The lines are guides to the eye.

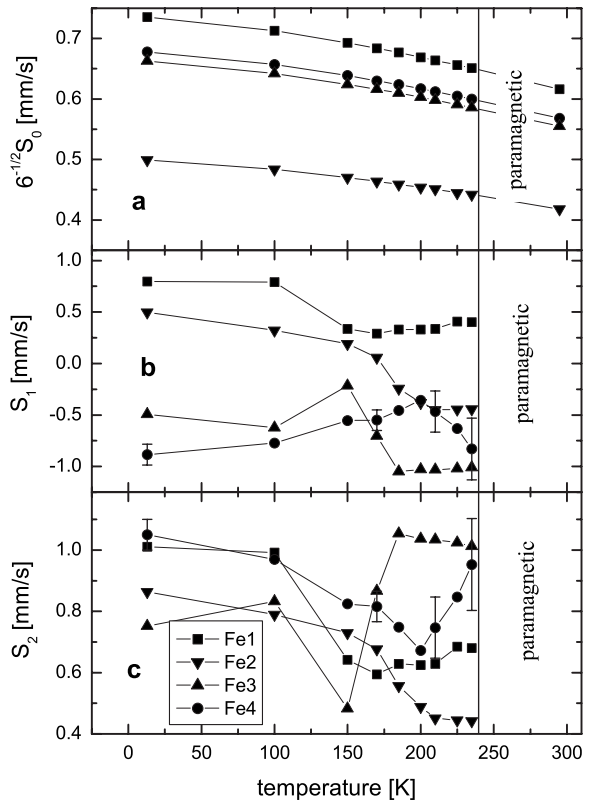

FIG. 4. Temperature dependence of invariants $6^{-1/2}S_0$, S_1, S_2 for different Fe sites. The lines in (b) and (c) are guides to the eye.

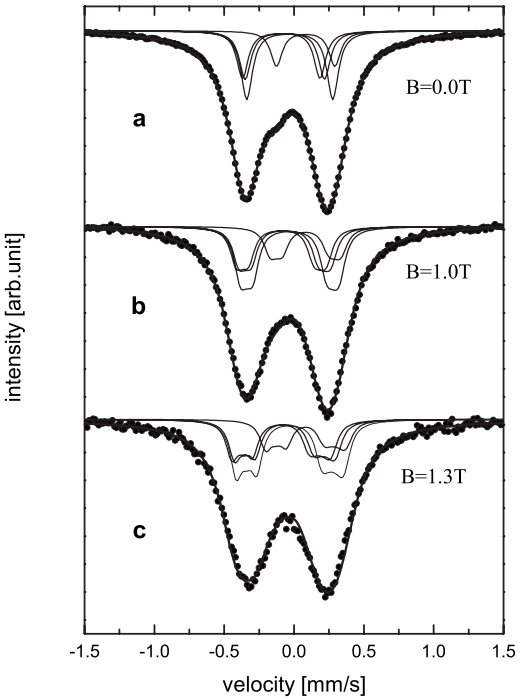

FIG. 5. The Mössbauer spectra measured at room temperature in the external magnetic field parallel to the gamma beam. The solid thick lines in (a) represent the best simultaneous fits for the first model from Sec. VIII. The solid thick lines in (b) and (c) represent the best fit using fixed values of invariants obtained in the simultaneous fit and assuming $\eta=0$ for all local iron sites. The experimental data for $B=0$ are the same as shown on the top of Fig. 2.

goes a transition to magnetic state at $T=155$ K. The hmf of the latter compound at 13 K equals 11 T and the iron magnetic moment inferred from neutron-diffraction measurements is $\mu_{Fe}=1.04\ \mu_B$.[31] So in this case the coupling constant is equal to 0.095 μ_B/T. Using this value, the estimated local Fe magnetic moments in UFe_5Sn are $\mu_{Fe1}=1.27\ \mu_B$, $\mu_{Fe2}=0.76\ \mu_B$, $\mu_{Fe3}=1.24\ \mu_B$, and $\mu_{Fe4}=1.41\ \mu_B$. Based on the value of the saturation magnetic moment per formula unit extrapolated to $T=0$ K and being equal to 5 μ_B,[20] occupations of the local sites by iron atoms, and taking also the assumption that the Fe moments are collinear, the uranium atom would acquire a magnetic moment of $\mu_U=-0.79\ \mu_B$. In other words, the direction of the uranium magnetic moments becomes opposite to the direction of the iron magnetic moments, as expected from the results given in Ref. 32.

The temperature dependence of invariants S_0, S_1, and S_2 are presented in Figs. 4(a)–4(c), respectively. The invariant S_0 reflects a $(1-A\cdot T^{3/2})$ dependence assumed above. The obtained value $A=(3.0\pm0.1)\times10^{-5}$ $K^{-3/2}$ confirms our assumption about the lattice dynamics' origin of the EFG temperature dependence. Indeed, recent *ab initio* calculations show that A is a positive constant in a range 10^{-4}–10^{-5} $K^{-3/2}$ and in many cases reproduces well the temperature dependence of the V_{zz}.[33] Values of the S_0 parameter for different Fe sites, similar to the IS, can be divided into two groups. The values observed for Fe2 have smaller values compared to those of the remaining sites. Moreover, the values for the sites with the same average volumetric constraints Fe1 and Fe3 show different values. It means that the value of the EFG reflects the symmetry of local surroundings rather than the distances and composition of the NN. The use of constraints for temperature dependence of some hyperfine parameters allow us to show that the singlelike doublet in the room-temperature spectrum, discussed in Sec. VI, should be considered as three components for Fe1, Fe3, and Fe4 sites with a similar value for parameter S_0, while this parameter for Fe2 differs clearly from those of the remaining Fe sites, as shown in Fig. 5(a) and Table II.

The invariants S_1 and S_2, which reflect an orientation of the hmf pseudovector in the PAS of the EFG, show a clear discontinuity around $T=170$ K for Fe3 sites [Figs. 4(b) and 4(c)]. This discontinuity is much more visible on the invariant S_2 than for S_1. This is correlated with a fast decrease in the value of the hmf. The behavior of the S_1 invariant of Fe2 shows relatively high amplitudes of change and also a change in the sign in the temperature range 170–200 K. The

TABLE II. Invariant $6^{-1/2}S_0$ and isomer shift (IS) from room-temperature measurement.

	$6^{-1/2}S_0$	IS (mm/s)
$S(1)$	0.62	-0.031 ± 0.005
$S(2)$	0.42	0.083 ± 0.005
$S(3)$	0.56	-0.092 ± 0.005
$S(4)$	0.57	-0.066 ± 0.005
D	0.54	-0.059 ± 0.005

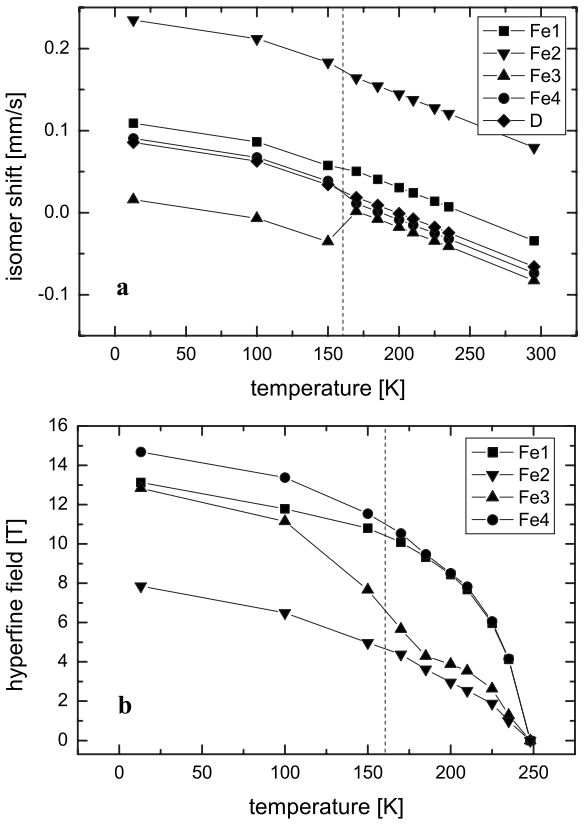

FIG. 6. The isomer shifts (a) and hyperfine magnetic fields (b) vs temperature. The second-order Doppler shift was calculated within the second model described in the text.

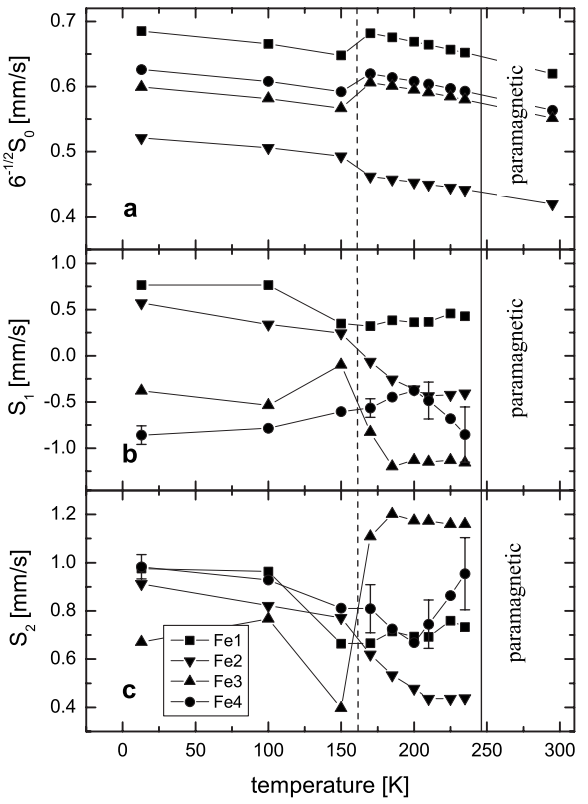

FIG. 7. Temperature dependence of invariants $6^{-1/2}S_0$, S_1, S_2 for different Fe sites assuming the possibility of a transition at a temperature of about 170 K. The lines are guides to the eye.

invariants for the remaining sites behave much more smoothly, although even these for Fe1 show a decrease but in the temperature between 150 and 170 K.

The invariants S_1 and S_2 can be determined only in the temperature range for which the hmf is nonzero. Thus, the increase of S_1 with a temperature for Fe4 at around $T=235$ K is, in our opinion, connected with an analysis of poorly resolved spectra and has no physical meaning. Since the temperature dependences of S_1 and S_2 indicate a sudden change around $T=170$ K, one has to consider a possibility of the phase transition and thus the change in the electronic structure. We have performed simultaneous fits under an assumption that is similar to that discussed at the beginning of this section, where the possibility of the temperature discontinuity in both the IS and EFG was allowed (in the vicinity of $T=170$ K). This was made in such a way that for every Fe surrounding a step function was used, e.g., for the center shift (CS) of the components: $\mathrm{CS}=\mathrm{SOD}(T)+\mathrm{IS}$ for $T<170$ K, while $\mathrm{CS}=\mathrm{SOD}(T)+\mathrm{IS}+\delta\mathrm{IS}$ for $T>170$ K, where δIS was an additional free parameter [see Fig. 6(a)]. Similarly, for the components of the EFG: $V_{ij}(T)=V_{ij}(0)(1-A\cdot T^{3/2})$ for $T<170$ K, while $V_{ij}(T)=[V_{ij}(0)+\delta V_{ij}](1-A\cdot T^{3/2})$ for $T>170$ K, where δV_{ij} were additional free parameters, see Fig. 7(a). This model fits slightly better for all the measured spectra, particularly in their central part. The obtained results of the IS and hmf are presented in Figs. 6(a) and 6(b), respectively. The behavior of the local hmf shows practically the same picture as that in the first model. It means that this parameter is not sensitive to the assumption about discontinuity. On the other hand, the behavior of the isomer shift [Fig. 6(a)] shows a distinct discontinuity for the Fe3 site, while those for the remaining sites are disturbed weakly. Within the scope of this model, the strong reduction of the Fe3 hmf is presumably associated with the change in the electronic structure, and also reflected in the IS at this site.

The temperature dependence of the S_0, S_1, and S_2 invariants is presented in Figs. 7(a)–7(c), respectively. As one can see, the possibility of the transition around 170 K is connected with the discontinuity of the S_0 invariant clearly visible on all iron sites. For the Fe2 site the invariant decreases crossing 170 K toward a higher temperature, while for the remaining sites the invariants increase. The results obtained for the invariants S_1 and S_2 do not differ much from the results found within the first model. So, the conclusions are the same as for the first model.

To recapitulate, the results presented above lead to the following conclusions:

(i) The hmf on Fe3 sites decreases with increasing temperature much faster than those on the remaining sites, and the fastest change takes place at around 170 K.

(ii) The discontinuity in the temperature dependence of the invariants S_1 and S_2 for the Fe3 sites is connected with a change of orientation of the magnetic moments of Fe3 with respect to the PAS.

(iii) The invariant S_0 reflects a $(1-A\cdot T^{3/2})$ dependence originating from lattice dynamics with the value $A=(3.0\pm0.1)\times10^{-5}$ $\mathrm{K}^{-3/2}$.

(iv) The electronic structure of the studied compound may change at around 170 K.

IX. IN EXTERNAL MAGNETIC-FIELD ROOM-TEMPERATURE MEASUREMENTS

In order to get the iron local invariants in the paramagnetic state, measurements in $B_{ext}=1$ T and 1.3 T external magnetic fields parallel to the gamma beam were carried out. The measured spectra are presented in Figs. 5(b) and 5(c). As one can see, the influence of the external magnetic field on the shape of the spectra is rather small. The spectra were analyzed according to the procedure given by Blaes *et al.*,[34] where random distribution of the EFG and the fixed direction of the hmf (B_{hf}) induced by an external magnetic field have been assumed. In principle, this kind of analysis can provide information about the local asymmetry parameter as well as the values of the local EFG. Unfortunately, because the applied field is too small with respect to the quadrupole interactions, the spectra presented in Figs. 5(b) and 5(c) are not well resolved, so the separation of these two quantities is a difficult task. Future experiments in higher external fields are needed in order to obtain these quantities. The solid thick lines in Fig. 5 represent the fits with invariants obtained by the method described in Sec. VII with the assumption of $\eta=0$ for all iron local surroundings. It should be stressed that only one free parameter, namely, the hmf, was used in the fit. As one can see, the theoretical curves fit well to the experimental points. However, the analysis reveals that the observed hyperfine fields are 0.61 T and 0.38 T for $B_{ext}=1.3$ T and 1 T, respectively. It means that the induced local hmf's are relatively large and directed antiparallel to the applied external field. This observation agrees well with the results of magnetization measurements, where one could detect a weak ferromagnetic component in the compound still existing at room temperature, i.e., fairly far above T_c.

X. CONCLUSIONS

High quality texture-free absorbers, prepared from a powdered UFe_5Sn single crystal and the use of a constrained invariant method, allowed us to interpret the shapes of the Mössbauer spectra at different temperatures, in terms of the contributions coming from separated Fe components. The theoretical intensities agree very well with the site occupancies resulting from the crystal structure. The presented method of invariants, dedicated for texture-free samples, may have potential application in material science and geology, where powdered absorbers are widely used.

Parameters of hyperfine interactions including hmf, IS, and invariants constructed from the EFG tensor and the hmf pseudovector for the ground state of UFe_5Sn were determined. These values could be directly compared with the results of electronic band-structure calculations. The proposed method of data treatment avoids any inconsistency caused by an ambiguity problem, although the hyperfine information is still incomplete.

Mössbauer spectra of UFe_5Sn measured at different temperatures show that all iron ions in the compound are paramagnetic at room temperature. The measurements carried out in the external magnetic field show that the hmf's observed on Fe nuclei are much smaller than those of an applied B_{ext}.

The temperature behavior of the hmf shows that the iron atoms order magnetically at $T=250$ K, indicating that the transition is mainly due to the ordering of the iron magnetic moments.

Our Mössbauer data imply that the transition observed in the magnetization data at $T\sim 180$ K is associated with a much faster decrease of hmf with temperature on Fe3 atoms (as compared with the behavior of the other local hmfs), and with the distinct change of the invariants S_1 and S_2 for Fe3, and likely for Fe2 sites.

The analysis of Fe at different sites—the spectrum measured at $T=13$ K—shows that the magnetic moments of Fe at different sites are linearly correlated with the number of NN iron atoms. Using a coupling constant derived from the UFe_4Al_8 compound,[31] the contribution of the iron magnetic moments to the spontaneous magnetization per formula unit was found to be $\mu=5.79\ \mu_B$, and the magnetic moments of uranium atoms are estimated to be $-0.79\ \mu_B$, which are antiparallel to the iron magnetic moments.

ACKNOWLEDGMENTS

The authors thank J. Cieśliński and A. P. Gonçalves for helpful discussions. The work was partially supported as a research project by the funds allocated for scientific research for the years 2008–2011.

APPENDIX

1. Lemma 1

Let $\boldsymbol{V}$ and $\boldsymbol{m}$ be a traceless, symmetric, real tensor, and a unit vector, respectively (both in R^3). Let us define p, q, and r according to Eqs. (1) and (4). Without losing generality, we may assume that $a=v_B=1$, because this results in simple scaling of all components of $\boldsymbol{V}$. There exists the traceless, symmetric, real tensor $\boldsymbol{\Omega}$ and the unit vector $\boldsymbol{n}$ for which equalities Eqs. (1) and (4) hold (upon replacement $\boldsymbol{V}\rightarrow\boldsymbol{\Omega}$ and $\boldsymbol{m}\rightarrow\boldsymbol{n}$) and $\boldsymbol{n}$ is perpendicular to one of the diagonal directions of $\boldsymbol{\Omega}$.

Proof

Without losing generality, we may choose $\boldsymbol{n}^T=(100)$. We will find an explicit form of the $\boldsymbol{\Omega}$. Let us assume that the diagonal direction is (001). Thus

$$\boldsymbol{\Omega}=\begin{bmatrix}\Omega_{11} & \Omega_{12} & 0\\ \Omega_{21} & \Omega_{22} & 0\\ 0 & 0 & -\Omega_{11}-\Omega_{22}\end{bmatrix}, \tag{A1}$$

then

$$\boldsymbol{n}^T\cdot\boldsymbol{\Omega}\cdot\boldsymbol{n}=\Omega_{11},$$

$$\boldsymbol{n}^T\cdot\boldsymbol{\Omega}^2\cdot\boldsymbol{n}=\Omega_{11}^2+\Omega_{12}\Omega_{21},$$

$$\mathrm{Tr}\ \boldsymbol{\Omega}^2 = 2\Omega_{11}^2 + 2\Omega_{22}^2 + 2\Omega_{11}\Omega_{22} + 2\Omega_{12}\Omega_{21}. \quad \text{(A2)}$$

Thus, using definition (2) and solving Eq. (A2), four solutions are obtained:

$$\Omega_{11} = \frac{-q}{16},$$

$$\Omega_{12} = \Omega_{21} = \pm \frac{1}{16}\sqrt{64 + 4p(8+p) - q^2 - 16r},$$

$$\Omega_{22} = \frac{1}{32}[q \pm \sqrt{q^2 - 16p(32+p) + 64(r-64)}]. \quad \text{(A3)}$$

Among these four solutions, there are two pairs. Each pair has the same eigenvalues and the eigenvectors, which differ by mirror reflection with respect to the *xy*, *xz*, or *yz* planes. Thus, Eq. (A3) is an explicit expression for the traceless, symmetric tensor $\boldsymbol{\Omega}$. Equation (A3) is real only when the expressions under square roots are not negative. Using abbreviations (1) and (4), these two conditions are equivalent to

$$\boldsymbol{m}^T \cdot \boldsymbol{V}^2 \cdot \boldsymbol{m} - (\boldsymbol{m}^T \cdot \boldsymbol{V} \cdot \boldsymbol{m})^2 \geq 0, \quad \text{(A4)}$$

$$(\boldsymbol{m}^T \cdot \boldsymbol{V} \cdot \boldsymbol{m})^2 + 2\ \mathrm{Tr}\ \boldsymbol{V}^2 - 4\boldsymbol{m}^T \cdot \boldsymbol{V}^2 \cdot \boldsymbol{m} \geq 0. \quad \text{(A5)}$$

Inequality (A4) follows from the properties of the scalar product. Indeed, for any two vectors $\boldsymbol{a}$ and $\boldsymbol{b}$, we have

$$a^2 b^2 \geq (\boldsymbol{a} \cdot \boldsymbol{b})^2. \quad \text{(A6)}$$

Let us take $\boldsymbol{a} = \boldsymbol{V} \cdot \boldsymbol{m}$, $\boldsymbol{b} = \boldsymbol{m}$. Inserting these $\boldsymbol{a}$ and $\boldsymbol{b}$ into Eq. (A6), we get Eq. (A4). Inequality (A5) is valid for any traceless Hermitian matrix in R^3, as a result of Lemma 2.

2. Lemma 2

For a traceless, Hermitian matrix $\boldsymbol{V}$ in R^3 and a unit vector $\boldsymbol{m}$, the following inequality holds:

$$(\boldsymbol{m}^T \cdot \boldsymbol{V} \cdot \boldsymbol{m})^2 + 2\ \mathrm{Tr}\ \boldsymbol{V}^2 - 4\boldsymbol{m}^T \cdot \boldsymbol{V}^2 \cdot \boldsymbol{m} \geq 0. \quad \text{(A7)}$$

Proof

Without losing generality we may choose a coordination system in which $\boldsymbol{m}$ will have only one nonzero coordinate, e.g., $\boldsymbol{m}^T = (1,0,0)$. In this system,

$$(\boldsymbol{m}^T \cdot \boldsymbol{V} \cdot \boldsymbol{m}) = V_{11},$$

$$(\boldsymbol{m}^T \cdot \boldsymbol{V}^2 \cdot \boldsymbol{m}) = V_{11}^2 + V_{12}V_{21} + V_{13}V_{31},$$

$$\mathrm{Tr}\ \boldsymbol{V}^2 = V_{11}^2 + V_{22}^2 + V_{33}^2 + 2(V_{12}V_{21} + V_{13}V_{31} + V_{23}V_{32}). \quad \text{(A8)}$$

Let us abbreviate:

$$F \equiv (\boldsymbol{m}^T \cdot \boldsymbol{V} \cdot \boldsymbol{m})^2 + 2\ \mathrm{Tr}\ \boldsymbol{V}^2 - 4\boldsymbol{m}^T \cdot \boldsymbol{V}^2 \cdot \boldsymbol{m}, \quad \text{(A9)}$$

thus

$$\begin{aligned} F &= V_{11}^2 + 2(V_{11}^2 + V_{22}^2 + V_{33}^2) + 4(V_{12}V_{21} + V_{13}V_{31} + V_{23}V_{32}) \\ &\quad - 4(V_{11}^2 + V_{12}V_{21} + V_{13}V_{31}) \\ &= (V_{22}^2 + V_{33}^2) - V_{11}^2 + 4V_{23}V_{32}. \end{aligned} \quad \text{(A10)}$$

For the traceless and Hermitian matrix

$$V_{11} = -(V_{22} + V_{33}) \quad \text{and} \quad V_{23}V_{32} \geq 0, \quad \text{(A11)}$$

hence,

$$F = (V_{22} - V_{33})^2 + 4V_{23}V_{32} \geq 0. \quad \text{(A12)}$$

[1] S. W. Karyagin, Fiz. Tverd. Tela (Leningrad) **8**, 493 (1966) [Sov. Phys. Solid State **8**, 391 (1966)].
[2] P. G. L. Williams and G. M. Bancroft, Moessbauer Eff. Methodol. **7**, 39 (1971).
[3] L. J. Dąbrowski, J. Piekoszewski, and J. Suwalski, Nucl. Instrum. Methods **91**, 93 (1971).
[4] L. J. Dąbrowski, J. Piekoszewski, and J. Suwalski, Nucl. Instrum. Methods **103**, 545 (1972).
[5] J. Dongen Torman, R. Jagannathan, and J. M. Trooster, Hyperfine Interact. **1**, 135 (1975).
[6] H. Spiering, Nucl. Instrum. Methods **154**, 295 (1978).
[7] G. K. Wertheim, Phys. Rev. **121**, 63 (1961).
[8] D. Barb, D. Tarina, A. Ito, and S. Morimoto, J. Phys. C **14**, 497 (1981).
[9] K. Szymański, Phys. Rep. **423**, 295 (2006).
[10] G. Le Caër and R. A. Brand, J. Phys.: Condens. Matter **10**, 10715 (1998).
[11] L. Dobrzyński, K. Szymański, and D. Satuła, Nukleonika **49**, S89 (2004).
[12] T. C. Gibb and N. N. Greenwood, *Mössbauer Spectroscopy* (Chapman and Hall, London, UK, 1971), pp. 63–72.
[13] K. Szymański, J. Phys.: Condens. Matter **12**, 7495 (2000).
[14] P. Zory, Phys. Rev. **140**, A1401 (1965).
[15] R. Ingalls, K. Ono, and L. Chandler, Phys. Rev. **172**, 295 (1968).
[16] R. Zimmermann, Nucl. Instrum. Methods **128**, 537 (1975).
[17] R. Zimmermann, Chem. Phys. Lett. **34**, 416 (1975).
[18] L. Häggström, University of Uppsala Report No. UUIP-851, 1974 (unpublished).
[19] O. C. Kistner and A. W. Sunyar, Phys. Rev. Lett. **4**, 412 (1960).
[20] A. P. Gonçalves, M. Godinho, and H. Noel, J. Solid State Chem. **154**, 551 (2000).
[21] A. P. Gonçalves, J. C. Waerenborgh, M. Almeida, M. Godinho, I. Catarino, G. Bonfait, and H. Noel, J. Magn. Magn. Mater. **260**, 473 (2003).
[22] R. Troć, C. Sułkowski, and H. Misiorek (to be published).
[23] S. Margulies and J. R. Ehrman, Nucl. Instrum. Methods **12**, 131 (1961).
[24] U. Bergmann, S. D. Shastri, D. P. Siddons, B. W. Batterman, and J. B. Hastings, Phys. Rev. B **50**, 5957 (1994).
[25] H. Akai, S. Blugel, R. Zeller, and P. H. Dederichs, Phys. Rev. Lett. **56**, 2407 (1986).
[26] J. C. Waerenborgh, A. P. Gonçalves, and M. Almeida, Solid State

Commun. **110**, 369 (1999).
[27] I. Vincze and A. T. Aldred, Phys. Rev. B **9**, 3845 (1974).
[28] B. Kolk, *Studies of Dynamical Properties of Solids with the Mössbauer Effect* (Elsevier Science, New York, 1984).
[29] V. H. Tran, R. Troć, J. Stepień-Damm, T. Komatsubara, F. Steglich, R. Hauser, and E. Bauer, Phys. Rev. B **66**, 054421 (2002).
[30] V. H. Tran, R. Troć, A. Czopnik, Z. Henkie, A. Jeżowski, D. Włosewicz, and F. Steglich, Acta Phys. Pol. B **34**, 1133 (2003).
[31] K. Rećko, M. Biernacka, L. Dobrzyński, K. Perzyńska, D. Satuła, K. Szymański, J. Waliszewski, W. Suski, K. Wochowski, G. Andre, and F. Bouree, J. Phys.: Condens. Matter **9**, 9541 (1997).
[32] A. Szajek and W. L. Malinowski, Phys. Status Solidi B **236**, 548 (2003).
[33] D. Torumba, K. Parlinski, M. Rots, and S. Cottenier, Phys. Rev. B **74**, 144304 (2006).
[34] N. Blaes, H. Fisher, and U. Gonser, Nucl. Instrum. Methods Phys. Res. B **9**, 201 (1985).